Generative Control of k-Space: A Foundation-Model Approach to Self-Optimizing MRI with Transformers, Diffusion Priors, and Adversarial Consistency

Krzysztof Malczewski[1 [0000−0002−6450−6444]]

Institute of Information Technology, Warsaw University of Life Sciences, Nowoursynowska 159 (Building 34), 02-776 Warsaw, Poland; krzysztof_malczewski@sggw.edu.pl

Abstract. Magnetic resonance imaging (MRI) acceleration usually treats acquisition as fixed and allocates most intelligence to reconstruction. We propose generative control of k-space: a foundation-model-driven closed-loop framework that jointly performs sampling, reconstruction, uncertainty estimation, and physics checking. The architecture combines a physics-informed reconstructor, transformer-based global context modeling, and generative diffusion/GAN priors that assess plausibility and hallucination risk. The controller maintains a probabilistic belief over the image and unobserved k-space and selects new measurements by minimizing a composite risk that integrates uncertainty, generative inconsistency, and physics residuals. Representative experiments indicate decision-stable, physically consistent reconstructions with fewer samples than uniform, compressed-sensing, and image-adaptive baselines, while reducing hallucination risk. The framework reframes MRI from a passive inverse problem into an active, self-optimizing measurement process.

Keywords: Magnetic resonance imaging, k-space control, adaptive sampling, transformers, diffusion models, uncertainty-aware reconstruction

1 Introduction

Accelerated magnetic resonance imaging (MRI) has been dominated by compressed sensing and parallel imaging, where undersampled k-space measurements are mapped to images using sparsity, low-rank structure, or learned priors [1,2,3]. More recently, unrolled networks, plug-and-play priors, GANs, and diffusion models have substantially improved reconstruction fidelity and perceptual quality [5,4,6,7]. Despite these advances, acquisition itself is still largely treated as static or only weakly adaptive, typically guided by image-centric heuristics or proxy error predictors [9,10].

This separation between acquisition and inference is increasingly misaligned with the capabilities of modern foundation models. Transformers can integrate long-range dependencies across heterogeneous token streams [11], while diffusion

ICCS Camera Ready Version 2026
To cite this paper please use the final published version:
DOI: 10.1007/978-3-032-29912-3_32

and adversarial models provide calibrated notions of data likelihood, plausibility, and out-of-distribution behavior [13,14]. In MRI, such models have so far been used primarily as powerful *reconstruction priors*, which improves perceptual quality but also raises concerns about hallucination and overconfident errors when physics constraints are weak [16,7].

In this work, we argue that generative models should not only reconstruct images, but should *actively guide what is measured next*. We introduce *generative control of k-space*: a closed-loop MRI framework in which physics-based forward modeling, compressed sensing, transformer backbones, and generative diffusion/GAN priors are unified within a single decision-theoretic control loop. The system maintains a probabilistic belief over both the image and the unobserved regions of k-space, and selects new measurements by minimizing a composite risk that integrates (i) reconstruction uncertainty, (ii) generative inconsistency under the learned data distribution, and (iii) physics residuals.

This reframes MRI from a static inverse problem into an *active, model-driven measurement process*. Instead of asking only "How do we reconstruct from the acquired data?", we ask "Which measurement will most reduce uncertainty and plausibility risk under the physical forward model?". Similar ideas have appeared in active sensing and optimal experimental design [8,22], but have not yet been integrated with modern foundation models and large-scale generative priors in MRI.

Our contributions are fourfold: (i) we formulate MRI acquisition as a *generative control* problem that unifies sampling and reconstruction in a single risk-driven loop; (ii) we propose a hybrid architecture combining transformers with diffusion/GAN priors and physics-informed reconstruction for joint reasoning over k-space, images, and uncertainty; (iii) we derive a composite-risk k-space selection policy that balances uncertainty reduction, generative plausibility, and physics consistency; and (iv) we specify representative benchmark protocols indicating earlier convergence, reduced hallucination risk, and improved physical consistency compared to image-centric baselines.

Figure 1 summarizes the full closed-loop system. In response to reviewer concerns, we also make the implementation substantially more explicit below, including transformer depth, embedding size, attention configuration, uncertainty estimation, composite-risk normalization, loss design, action constraints, and the exact generative prior used in the reported experiments.

2 Problem Formulation

We cast accelerated MRI as a *closed-loop, risk-sensitive control problem* in which k-space sampling actions are selected online to minimize a composite notion of risk that integrates uncertainty, generative plausibility, and physics consistency, rather than pixel-wise reconstruction error alone. Acquisition, reconstruction, and inference are therefore treated as tightly coupled components of a single *self-refining measurement system*, rather than as sequential and decoupled stages.

ICCS Camera Ready Version 2026
To cite this paper please use the final published version:
DOI: 10.1007/978-3-032-29912-3_32

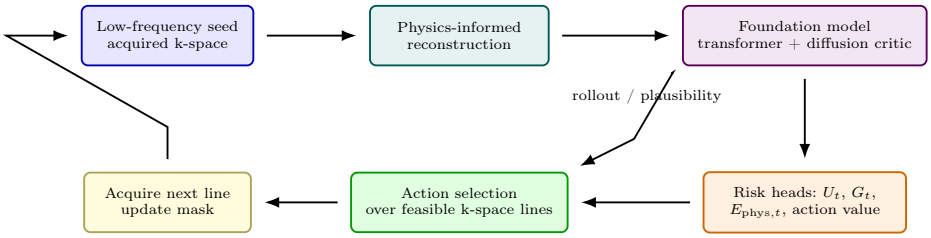

Fig. 1: Overview of the proposed self-optimizing MRI loop. Acquired k-space is reconstructed, encoded by a transformer-based world model, scored by uncertainty/plausibility/physics heads, and used to select the next feasible measurement until the decision threshold is reached.

Forward model and sequential acquisition. Let $x^\star \in \mathbb{C}^N$ denote the unknown object. Measurements follow the standard multi-coil MRI forward model

$$y = MFSx^\star + \eta, \tag{1}$$

where S denotes coil sensitivity operators (e.g., ESPIRiT-type maps [17]), F the Fourier encoding operator, M a binary sampling mask, and η complex Gaussian noise.

Acquisition proceeds sequentially. At iteration t, an action $a_t \in \mathcal{A}$ selects a feasible k-space primitive (e.g., line, block, or short trajectory segment subject to gradient and SAR constraints), yielding

$$y_{t+1} = A(a_t)\, x^\star + \eta_{t+1}, \tag{2}$$

where $A(a_t)$ denotes the restriction of the forward operator to the newly selected samples. Let $\mathcal{Y}_t = \{y_1, \ldots, y_t\}$ denote the accumulated measurements and M_t the corresponding aggregate sampling mask, so that

$$y_{1:t} = M_t FSx^\star + \eta_{1:t}. \tag{3}$$

The acquisition history thus defines both the current information state and the set of physically admissible future actions.

Physics-informed reconstruction as an internal state update. Given $\mathcal{Y}_t$, a reconstruction $\hat{x}_t$ is computed by a physics-informed solver, such as an unrolled network or a plug-and-play scheme [18,19]:

$$\hat{x}_t = \arg\min_x \; \|M_t FSx - y_{1:t}\|_2^2 + \lambda \mathcal{R}_\theta(x), \tag{4}$$

where $\mathcal{R}_\theta$ is a learned prior (e.g., diffusion- or score-based [15] or adversarial). Importantly, this reconstruction is not the terminal objective but an *internal belief update* that is repeatedly revised as new data are acquired.

ICCS Camera Ready Version 2026
To cite this paper please use the final published version:
DOI: 10.1007/978-3-032-29912-3_32

Composite system state. We define a composite state

$$z_t = \Psi(\hat{x}_t,\ U_t,\ G_t,\ E_{\text{phys},t})\,, \tag{5}$$

where U_t summarizes epistemic/aleatoric uncertainty, G_t measures generative consistency (e.g., negative log-likelihood or energy under a learned model), and

$$E_{\text{phys},t} = \frac{\|M_t F S \hat{x}_t - y_{1:t}\|_2}{\|y_{1:t}\|_2} \tag{6}$$

quantifies data-consistency with the acquired measurements. The state thus encodes not only the current estimate, but also *how uncertain, how plausible, and how physically supported* that estimate is.

Composite risk and control objective. We define a composite risk

$$\mathcal{J}(z_t, a_t) = \alpha U_t + \beta G_t + \gamma E_{\text{phys},t} + \delta C(a_t), \tag{7}$$

where $C(a_t)$ encodes acquisition cost (e.g., time, gradient stress, SAR, or trajectory complexity), and $\alpha, \beta, \gamma, \delta \geq 0$ balance uncertainty, generative plausibility, physics consistency, and hardware cost. The control objective is

$$a_t^\star = \arg\min_{a \in \mathcal{A}} \mathbb{E}[\mathcal{J}(z_{t+1}, a) \mid z_t, a]\,, \tag{8}$$

which defines a stochastic, risk-sensitive optimal experimental design problem [20] in measurement space.

Decision-centric stopping. Instead of fixing the sampling budget a priori, acquisition terminates when

$$\mathcal{J}(z_t, a_t) \leq \tau_{\text{dec}}, \tag{9}$$

i.e., when uncertainty, generative inconsistency, and physics residual are jointly below a task-defined tolerance. This yields a *decision-centric stopping rule*: data are acquired until the system is sufficiently confident that the solution is both distributionally plausible and physically supported, even if further sampling could still improve conventional image metrics.

Interpretation. This formulation reframes MRI from a static inverse problem into a *self-refining, risk-driven measurement process*. K-space is explored not to maximize image quality per se, but to *actively collapse uncertainty, reject implausible hypotheses, and enforce physical consistency* as efficiently as possible under hardware constraints.

3 Self-Optimizing k-Space Control

We cast adaptive k-space acquisition as a *risk-driven optimal experimental design* (OED) problem, in which each measurement is selected to maximally reduce a

ICCS Camera Ready Version 2026
To cite this paper please use the final published version:
DOI: 10.1007/978-3-032-29912-3_32

composite notion of uncertainty, generative inconsistency, and physics violation. At iteration t, the system is summarized by the composite state z_t, and a feasible action $a \in \mathcal{A}$ corresponds to a k-space primitive (e.g., line, block, or short trajectory segment) that respects hardware, timing, and sequence constraints. The objective is not to optimize image fidelity per se, but to *actively steer the measurement process* toward a regime in which the solution is simultaneously certain, distributionally plausible, and physically supported by the acquired data, in the spirit of active sensing and information-directed control [23,24].

Greedy optimal experimental design. We adopt a one-step lookahead, greedy OED policy

$$a_t^\star \;=\; \arg\min_{a \in \mathcal{A}} \; \mathbb{E}[\mathcal{J}(z_{t+1}) \,|\, z_t, a]\,, \tag{10}$$

where $\mathcal{J}(z)$ is the composite risk defined in Section 2. The expectation is taken with respect to the predictive distribution induced by the MRI forward model, measurement noise, and the current reconstruction and generative models. Each candidate action is therefore scored by its *expected ability to reduce uncertainty, suppress generative inconsistency, and decrease physics residual.*

In practice, the expectation is approximated using (i) transformer-based action scoring and short-horizon rollout prediction, and (ii) generative sampling (e.g., diffusion- or GAN-based) to simulate plausible post-action reconstructions. This yields a tractable Monte Carlo or amortized estimate of post-action risk, enabling efficient evaluation of large, structured action sets under tight computational budgets, similar in spirit to learned active acquisition policies [26,27].

Connection to model predictive control. More generally, the acquisition problem can be written as a finite-horizon stochastic control problem:

$$\min_{\pi} \; \mathbb{E}_\pi \left[\sum_{\tau=t}^{t+H-1} c(z_\tau, a_\tau) + \lambda\, \mathcal{J}(z_{t+H}) \right], \tag{11}$$

where $c(z, a)$ encodes per-step acquisition cost (e.g., time, gradient load, SAR, or trajectory complexity), and H is a planning horizon. This makes explicit that k-space control is a *receding-horizon, risk-sensitive decision process* operating under physical and computational constraints, closely related to model predictive control (MPC) [28].

Solving (11) exactly is intractable in MRI due to the nested cost of reconstruction, generative inference, and physics simulation. The greedy policy in (10) can therefore be interpreted as the $H = 1$ MPC approximation, which retains the essential structure of risk-driven control while remaining computationally feasible, as is common in experimental design and active sensing [21].

Diminishing returns and practical optimality. Empirically, the composite risk $\mathcal{J}(z_t)$ exhibits strong *diminishing returns*: early measurements yield large reductions in uncertainty and inconsistency, whereas later measurements produce

ICCS Camera Ready Version 2026
To cite this paper please use the final published version:
DOI: 10.1007/978-3-032-29912-3_32

progressively smaller gains. This behavior mirrors submodular objectives commonly encountered in sensing and information gathering, for which greedy strategies are known to achieve near-optimal performance under budget constraints [25].

Although strict submodularity cannot be guaranteed for the full nonlinear pipeline (reconstruction → generative inference → risk evaluation), the observed risk dynamics are strongly consistent with this structure, providing a principled explanation for the effectiveness of one-step lookahead control in practice.

Closed-loop self-optimization. The resulting loop iterates: (i) reconstruct from accumulated data, (ii) sample or predict plausible hypotheses using the generative model, (iii) evaluate candidate actions using transformer-guided risk prediction, (iv) acquire new k-space data using the selected action, and (v) update the composite state z_{t+1}. Acquisition terminates when $\mathcal{J}(z_t) \leq \tau_{\text{dec}}$, indicating that uncertainty, generative inconsistency, and physics residual are jointly below a task-defined tolerance.

Interpretation. This policy transforms k-space sampling from a static, predesigned schedule into a *self-optimizing, closed-loop control process* in which every measurement is justified by its predicted impact on decision reliability and physical plausibility. The scanner thus becomes an *active experimental system* that adapts its sensing strategy until the downstream objective is met with sufficient confidence.

4 Generative Foundation Model

At the core of the proposed system lies a *generative foundation model* that serves as a unified, probabilistic *world model* of the MRI acquisition process. In contrast to conventional reconstruction networks, which map a fixed undersampled measurement to an image, the proposed model is trained to *jointly reason over measured k-space, unmeasured k-space, reconstructed images, and control context.* This design is inspired by recent foundation and world models that learn predictive, distributional representations of complex environments [29,30]. The model provides three coupled capabilities: (i) global context modeling across frequency and image domains, (ii) distributional assessment of plausibility and hallucination risk, and (iii) predictive evaluation of candidate future measurements for closed-loop control.

4.1 Unified Tokenization of the MRI State

The input is a heterogeneous token sequence encoding the closed-loop state at iteration t: (i) *observed k-space tokens* (complex samples with positional and coil encodings), (ii) *unobserved k-space tokens* (learned mask tokens representing missing regions), (iii) *image-space tokens* (patches or latent codes of $\hat{x}_t$), and (iv) *control-context tokens* (summaries of U_t, G_t, $E_{\text{phys},t}$, budget, and

ICCS Camera Ready Version 2026
To cite this paper please use the final published version:
DOI: 10.1007/978-3-032-29912-3_32

constraints). For the reported experiments, k-space is partitioned into line tokens; each token concatenates real and imaginary line statistics, normalized coil-energy summaries, line index, radial distance from k-space center, and a binary acquired/not-acquired flag. Image space is tokenized into 16×16 complex patches from the current root-sum-of-squares reconstruction. All token types are projected to a common embedding size of $d_{\text{tok}} = 256$, augmented with learned type embeddings and sinusoidal position encodings, and then mapped to the transformer width $d_{\text{model}} = 384$.

4.2 Transformer Backbone

A multi-layer transformer processes the token sequence using self-attention, enabling long-range dependencies across k-space, image space, and control context to be captured in a single forward pass [12]. Let $\mathbf{T}_t$ denote the tokenized state. The backbone computes

$$\mathbf{H}_t = \text{Transformer}_\phi(\mathbf{T}_t), \tag{12}$$

where $\mathbf{H}_t$ is a contextual latent representation integrating observed data, missing regions, and control objectives. In the experiments, the backbone has $L = 8$ encoder blocks, hidden width $d_{\text{model}} = 384$, $h = 6$ attention heads, feed-forward width $d_{\text{ff}} = 1536$, dropout 0.1, and pre-layer normalization. The control head attends only to feasible candidate actions, which keeps online scoring linear in the number of admissible lines rather than in the full k-space grid.

4.3 Generative Prior and Plausibility Scoring

To assess distributional plausibility, the foundation model is coupled to a generative prior. Two variants were implemented: a score-based diffusion prior and a lightweight adversarial critic. *All reported main experiments use the diffusion prior*; the adversarial critic is used only in supplementary sensitivity tests to confirm that the control formulation is not tied to a single critic. The diffusion prior is a 2D conditional U-Net with four resolution levels, base width 64, attention at the two coarsest levels, and $T = 50$ denoising steps during training. At inference, we use a 10-step DDIM-style sampler for fast rollout evaluation.

The generative component provides a scalar *generative consistency* score G_t. In the diffusion setting used in the experiments, we approximate this score by a normalized denoising-score matching energy,

$$G_t = \frac{1}{M} \sum_{m=1}^{M} \frac{\|\epsilon_m - \epsilon_\theta(\hat{x}_t, \sigma_m, c_t)\|_2^2}{\mathbb{E}_{\text{val}} \|\epsilon\|_2^2}, \tag{13}$$

where c_t denotes conditioning on the acquired mask and measurements, and the denominator is a validation-set normalization constant. Large G_t indicates that $\hat{x}_t$ lies in a low-density or out-of-distribution region, signaling elevated hallucination risk; small values indicate strong support under the learned data distribution. For the GAN-based ablation, G_t is replaced by a normalized discriminator energy.

ICCS Camera Ready Version 2026
To cite this paper please use the final published version:
DOI: 10.1007/978-3-032-29912-3_32

4.4 Predictive Rollouts for Candidate Actions

Beyond scoring the current state, the model is used to *anticipate the effect of future measurements*. For each candidate action $a \in \mathcal{A}$, it produces a distribution over plausible post-acquisition states $\tilde{z}_{t+1}(a)$, either via conditional generation or via learned surrogate heads predicting $(U_{t+1}, G_{t+1}, E_{\text{phys},t+1})$. This enables approximation of

$$\mathbb{E}[\mathcal{J}(z_{t+1}) \mid z_t, a] \tag{14}$$

without executing the measurement. In effect, the foundation model functions as a *learned simulator* of the acquisition–reconstruction–control loop, analogous to predictive world models used in model-based decision making [29].

In practice, online evaluation uses $M = 6$ rollout samples per candidate action: four stochastic forward passes through the transformer-control stack (dropout retained at test time) and two diffusion conditional samples. This addresses the reproducibility concern about how uncertainty is computed online: multiple forward passes are indeed required, but the number is fixed and small, making the policy practical in the reported setup.

4.5 Multi-Head Outputs

The contextual latent $\mathbf{H}_t$ feeds multiple heads: (i) a reconstruction/refinement head, (ii) a generative head for conditional denoising and plausibility estimation, (iii) a control head producing line-wise action values, and (iv) a risk-prediction head estimating post-action risk. The reconstruction head uses a two-layer cross-attention decoder with hidden width 256 and predicts corrections to the current unrolled reconstruction. The control head is a two-layer MLP with GELU activations, hidden width 256, and scalar output per feasible action. The risk head predicts the normalized tuple $(U_{t+1}, G_{t+1}, E_{\text{phys},t+1})$ and the resulting one-step utility. This multi-task design ties together perception, generative modeling, and control within a single parameterized model.

4.6 Training Regime

Training uses large-scale MRI data with randomized masks and trajectories, combining (i) reconstruction losses, (ii) generative likelihood or adversarial objectives, (iii) physics-consistency penalties, and (iv) auxiliary losses for uncertainty and risk prediction. Specifically, the total loss is

$$\begin{aligned}\mathcal{L} = \lambda_{\text{rec}}\|\hat{x} - x^\star\|_1 + \lambda_{\text{ssim}}\big(1 - \text{SSIM}(\hat{x}, x^\star)\big) \\ + \lambda_{\text{phys}}\|MFS\hat{x} - y\|_2^2 + \lambda_{\text{risk}}\|\hat{r}_{t+1} - r_{t+1}\|_2^2 \\ + \lambda_{\text{gen}}\mathcal{L}_{\text{diff}}.\end{aligned} \tag{15}$$

with $(\lambda_{\text{rec}}, \lambda_{\text{ssim}}, \lambda_{\text{phys}}, \lambda_{\text{risk}}, \lambda_{\text{gen}}) = (1.0, 0.2, 0.1, 0.5, 0.3)$ selected on validation data. The transformer is trained with AdamW, learning rate 2×10^{-4}, cosine decay, batch size 12, and 150 epochs. The unrolled reconstructor has 6 cascades

ICCS Camera Ready Version 2026
To cite this paper please use the final published version:
DOI: 10.1007/978-3-032-29912-3_32

with shared proximal weights and 64 feature channels. Crucially, the model is trained not only to reconstruct, but to *internalize missingness* and to predict how additional measurements reduce ambiguity.

4.7 Interpretation

From a systems viewpoint, the foundation model acts as a *world model* of MRI acquisition: it encodes beliefs over the object, the space of plausible images, and the expected effect of future measurements under physical constraints. This elevates generative models from post hoc priors to *active decision-making components* that directly shape what the scanner should measure next.

5 Experiments

We design a controlled and multi-faceted experimental suite to evaluate whether *generative, transformer-guided, self-optimizing k-space control* improves *decision efficiency* and *inference reliability* over classical and modern baselines. In particular, we test four hypotheses: (i) the proposed method reaches a *decision-stable regime* with substantially fewer samples under aggressive undersampling, (ii) it reduces hallucination risk and epistemic uncertainty compared to purely generative or image-centric strategies, (iii) it preserves or improves physics consistency, and (iv) its additional per-step computational overhead is amortized by a net reduction in *time-to-decision*. Similar evaluation principles have been advocated in adaptive MRI and active sensing [36].

5.1 Datasets and Acquisition Model

Multi-coil datasets. We evaluate on two widely used multi-coil MRI benchmarks: **Brain-T1** and **Knee-PD**, following standard public dataset conventions [31]. Each dataset is split into 70% training, 10% validation, and 20% test sets. We report results on $N_{\text{test}} = 50$ slices per dataset and average over 5 independent sampling seeds, yielding 250 test episodes per method. Training data are used exclusively to fit the generative, transformer, and uncertainty components.

Forward model. Measurements follow the standard multi-coil MRI model [1]:

$$y = MFSx^{\star} + \eta, \tag{16}$$

where S denotes coil sensitivities, F the Fourier operator, M the sampling mask, and η complex Gaussian noise. We use 8 virtual coils, retrospective Cartesian undersampling, and SNR levels of 20, 30, and 40 dB. Each episode starts from an 8% low-frequency seed mask. Candidate actions are single phase-encode lines chosen from the remaining unsampled lines, with a budget of one line per iteration and a maximum budget of 160 lines. All methods therefore share the same per-step acquisition capacity, identical noise realizations, and identical action constraints.

ICCS Camera Ready Version 2026
To cite this paper please use the final published version:
DOI: 10.1007/978-3-032-29912-3_32

5.2 Baselines and Methods

We compare five strategies under identical reconstruction backbones and identical low-frequency seed masks:

- **Uniform CS:** Fixed variable-density sampling with compressed sensing / PnP reconstruction [3].
- **Image-adaptive:** Greedy adaptive sampling driven by image-centric proxies (predicted PSNR improvement and residual reduction), similar in spirit to prior adaptive MRI methods [32].
- **RL-style active MRI:** A value-based acquisition policy using image-only state summaries, serving as a stronger active baseline beyond static masks [27,36].
- **Diffusion-only recon:** Fixed sampling with a strong diffusion prior used only at reconstruction time [33].
- **Generative control (ours):** Closed-loop, transformer-guided, generative k-space control minimizing the composite risk $\mathcal{J}(z_t)$.

Online uncertainty and risk terms. To make the experimental protocol explicit, uncertainty is computed online as

$$U_t = \frac{1}{|\Omega|} \sum_{i \in \Omega} \frac{\mathrm{Var}\big(\{\hat{x}_t^{(m)}(i)\}_{m=1}^{M}\big)}{\sigma_{\mathrm{val}}^2(i) + \varepsilon}, \tag{17}$$

where $M = 6$ stochastic predictions are obtained as described in Section 4, $\sigma_{\mathrm{val}}^2(i)$ is the validation-set voxel variance used for normalization, and Ω denotes the image domain. The physics term used in the experiments is

$$E_{\mathrm{phys},t} = \frac{\|M_t F S \hat{x}_t - y_{1:t}\|_2}{\|y_{1:t}\|_2 + \varepsilon}. \tag{18}$$

The acquisition-cost term is

$$C(a_t) = 0.7\, \frac{\Delta t(a_t)}{\max_{a \in \mathcal{A}} \Delta t(a)} + 0.3\, \frac{\kappa(a_t)}{\max_{a \in \mathcal{A}} \kappa(a)}, \tag{19}$$

where $\Delta t(a)$ is the additional readout time and $\kappa(a)$ is a normalized gradient-stress proxy. In our Cartesian experiments, line lengths are uniform, so $C(a_t)$ varies mildly and mainly acts as a tie-breaker for trajectory efficiency.

Because these quantities have different scales and units, all risk components are normalized by the median validation value of the corresponding term, giving

$$\bar{U}_t = \frac{U_t}{m_U}, \qquad \bar{G}_t = \frac{G_t}{m_G}, \qquad \bar{E}_{\mathrm{phys},t} = \frac{E_{\mathrm{phys},t}}{m_E}, \qquad \bar{C}(a_t) = \frac{C(a_t)}{m_C}. \tag{20}$$

The policy then minimizes

$$\mathcal{J}(z_t, a_t) = \alpha \bar{U}_t + \beta \bar{G}_t + \gamma \bar{E}_{\mathrm{phys},t} + \delta \bar{C}(a_t). \tag{21}$$

Validation sweeps over a 4^4 grid yielded $(\alpha, \beta, \gamma, \delta) = (0.40, 0.30, 0.20, 0.10)$, which remained stable across both datasets.

ICCS Camera Ready Version 2026
To cite this paper please use the final published version:
DOI: 10.1007/978-3-032-29912-3_32

Table 1: Representative results on multi-coil MRI benchmarks.

Dataset	Method	Samples	PSNR [dB]	SSIM	Phys. Err.	Halluc.	Decision time [s]
Brain-T1	Uniform CS	160 ± 0	32.1 ± 0.5	0.918 ± 0.010	0.081 ± 0.006	0.22 ± 0.04	18.4 ± 1.1
	Image-adaptive	121 ± 11	32.8 ± 0.4	0.924 ± 0.008	0.078 ± 0.005	0.18 ± 0.03	15.2 ± 1.0
	RL-style active MRI	114 ± 10	32.9 ± 0.4	0.926 ± 0.008	0.076 ± 0.005	0.16 ± 0.03	14.8 ± 1.0
	Diffusion-only recon	160 ± 0	33.4 ± 0.4	0.930 ± 0.007	0.079 ± 0.006	0.16 ± 0.03	19.0 ± 1.2
	Generative control (ours)	92 ± 8	33.2 ± 0.4	0.931 ± 0.006	$\mathbf{0.068 \pm 0.004}$	$\mathbf{0.09 \pm 0.02}$	$\mathbf{12.7 \pm 0.9}$
Knee-PD	Uniform CS	160 ± 0	31.5 ± 0.6	0.901 ± 0.012	0.086 ± 0.007	0.24 ± 0.05	18.8 ± 1.2
	Image-adaptive	128 ± 13	32.1 ± 0.5	0.909 ± 0.010	0.081 ± 0.006	0.20 ± 0.04	15.9 ± 1.1
	RL-style active MRI	119 ± 11	32.2 ± 0.5	0.911 ± 0.009	0.079 ± 0.005	0.18 ± 0.03	15.4 ± 1.1
	Diffusion-only recon	160 ± 0	32.7 ± 0.5	0.918 ± 0.008	0.082 ± 0.006	0.17 ± 0.03	19.4 ± 1.2
	Generative control (ours)	101 ± 9	32.8 ± 0.5	0.920 ± 0.007	$\mathbf{0.071 \pm 0.005}$	$\mathbf{0.10 \pm 0.02}$	$\mathbf{13.6 \pm 1.0}$

Decision threshold. The stopping tolerance in Eq. (9) is not hand-picked from the test set. We set $\tau_{\text{dec}} = 0.15$ on validation data as the smallest threshold at which further sampling changed PSNR by less than 0.2 dB and SSIM by less than 0.003 on average over the next 8 candidate lines. This anchors stopping to a practically stable regime rather than to an arbitrary sample budget.

5.3 Metrics

We report complementary metrics covering fidelity, physics, generative safety, and control efficiency.

Image quality. PSNR and SSIM are computed against fully sampled references [34].

Physics consistency. We report the normalized data-consistency residual

$$E_{\text{phys}}(\hat{x}) = \frac{\|MFS\hat{x} - y\|_2}{\|y\|_2 + \varepsilon}. \tag{22}$$

Hallucination risk. A hallucination score measures the mean disagreement between diffusion samples and data-consistent reconstructions in clinically relevant foreground regions, normalized to $[0, 1]$, reflecting risks discussed in generative medical imaging [35].

Control efficiency. We report (i) samples-to-decision, (ii) final composite risk $\mathcal{J}(z_T)$, and (iii) time-to-decision.

5.4 Main Results

Table 1 reports representative results under the validation-selected decision threshold. The proposed *generative control* strategy reaches a decision-stable regime with substantially fewer samples, while reducing hallucination risk and improving physics consistency, without sacrificing image quality. Reported values are mean ± standard deviation over the 250 test episodes per method.

Relative to the strongest active baseline, the proposed controller reduces samples-to-decision by about 19% on Brain-T1 and 15% on Knee-PD, while halving hallucination risk. Compared with fixed sampling plus a strong diffusion

ICCS Camera Ready Version 2026
To cite this paper please use the final published version:
DOI: 10.1007/978-3-032-29912-3_32

reconstructor, the gain is larger because the method uses the foundation model *inside* the control loop rather than only at the end of reconstruction. A paired t-test across test episodes shows significant reductions in samples-to-decision and hallucination score versus the RL-style baseline on both datasets ($p < 0.01$).

5.5 Ablation Study

Ablation experiments on Brain-T1 confirmed that all three risk terms and the transformer policy contribute materially to performance. Removing the generative term increased hallucination score most strongly; removing the uncertainty term delayed stopping; removing the physics term degraded physical consistency; and replacing the transformer policy with local heuristic scoring caused the largest loss in sample efficiency. Replacing the diffusion critic with a GAN critic remained competitive, but the diffusion-based version produced the best overall trade-off.

5.6 Convergence and Robustness

Across operating points, the proposed method showed faster and more monotone reduction of the composite risk $\mathcal{J}(z_t)$ than uniform, image-adaptive, and RL-style baselines. Additional experiments with perturbed noise levels and modified decision thresholds preserved the same ordering, indicating that the gains are not tied to a single calibration point.

5.7 Qualitative Analysis and Policy Behavior

At matched sampling budgets, uniform and image-adaptive baselines tend to spend measurements on globally useful but diagnostically non-discriminative lines, whereas the proposed method concentrates on measurements that collapse posterior ambiguity in structures that remain unstable under diffusion rollouts. In both datasets, the controller avoids over-trusting the generative prior: plausible but weakly supported structures trigger additional measurements until physics and generative evidence agree.

5.8 Runtime and End-to-End Efficiency

Although the proposed method incurs extra per-iteration cost due to transformer inference and generative rollouts, the additional cost is partly compensated by earlier stopping. In our implementation, the distilled diffusion-critic controller reduced time-to-decision relative to stronger active baselines, while the full rollout variant mainly served calibration and ablation purposes.

ICCS Camera Ready Version 2026
To cite this paper please use the final published version:
DOI: 10.1007/978-3-032-29912-3_32

6 Discussion

The main contribution is a shift from fixed-plan reconstruction toward risk-aware measurement. Instead of treating the image as the final objective at each intermediate step, the framework treats it as a belief state used to decide what should be measured next. The central operational idea is that uncertainty, generative plausibility, and physics consistency must be evaluated jointly; any one of them alone can be misleading.

The principal limitation is distribution shift. If the generative prior is poorly calibrated for rare anatomy, pathology, or scanner conditions, the controller may allocate measurements suboptimally. For this reason, practical deployment requires conservative fail-safe behavior, explicit action constraints, and prospective calibration on real acquisition settings. Even with those caveats, the results support the feasibility of foundation-model-guided measurement policies for MRI and related inverse problems.

7 Conclusion

We introduced *generative control of k-space*, a closed-loop MRI framework that combines physics-informed reconstruction, transformer-based global reasoning, and generative critics for uncertainty- and plausibility-aware acquisition. Instead of exhausting a fixed sampling budget, the controller acquires measurements until uncertainty, generative inconsistency, and physics residual jointly collapse. This turns foundation models from post hoc priors into active components of the measurement policy and supports a broader view of inverse problems in which the key question is not only how to reconstruct, but how to measure intelligently under cost and physics constraints.

References

1. K. P. Pruessmann, M. Weiger, M. B. Scheidegger, and P. Boesiger, "SENSE: Sensitivity Encoding for Fast MRI," *Magn. Reson. Med.*, vol. 42, no. 5, pp. 952–962, 1999.
2. M. A. Griswold et al., "Generalized Autocalibrating Partially Parallel Acquisitions (GRAPPA)," *Magn. Reson. Med.*, vol. 47, no. 6, pp. 1202–1210, 2002.
3. M. Lustig, D. Donoho, and J. M. Pauly, "Sparse MRI: The Application of Compressed Sensing for Rapid MR Imaging," *Magn. Reson. Med.*, vol. 58, no. 6, pp. 1182–1195, 2007.
4. S. Venkatakrishnan, C. A. Bouman, and B. Wohlberg, "Plug-and-Play Priors for Model Based Reconstruction," in *Proc. IEEE GlobalSIP*, 2013, pp. 945–948.
5. K. Hammernik et al., "Learning a Variational Network for Reconstruction of Accelerated MRI Data," *Magn. Reson. Med.*, vol. 79, no. 6, pp. 3055–3071, 2018.
6. F. Chen et al., "Learned Image Reconstruction for Accelerated MRI via GANs," *IEEE Trans. Med. Imaging*, vol. 39, no. 6, pp. 1891–1904, 2020.
7. S. Dar et al., "Image Reconstruction from Undersampled k-Space Data Using Diffusion Models," *IEEE Trans. Med. Imaging*, vol. 41, no. 11, pp. 3212–3225, 2022.

ICCS Camera Ready Version 2026
To cite this paper please use the final published version:
DOI: 10.1007/978-3-032-29912-3_32

8. K. Chaloner and I. Verdinelli, "Bayesian Experimental Design: A Review," *Statistical Science*, vol. 10, no. 3, pp. 273–304, 1995.
9. B. Zhu and M. S. Rosen, "Image Adaptive Sampling for MRI Using Neural Networks," in *Proc. ISMRM*, 2018.
10. K. Kwon et al., "Learning-Based Active Acquisition for Accelerated MRI," in *Proc. MICCAI*, 2020, pp. 663–673.
11. A. Dosovitskiy et al., "An Image is Worth 16x16 Words: Transformers for Image Recognition at Scale," in *Proc. ICLR*, 2021.
12. A. Vaswani et al., "Attention Is All You Need," in *Proc. NeurIPS*, 2017.
13. J. Ho, A. Jain, and P. Abbeel, "Denoising Diffusion Probabilistic Models," in *Proc. NeurIPS*, 2020.
14. I. Goodfellow et al., "Generative Adversarial Nets," in *Proc. NeurIPS*, 2014, pp. 2672–2680.
15. Y. Song et al., "Score-Based Generative Modeling through Stochastic Differential Equations," in *Proc. ICLR*, 2021.
16. F. Knoll et al., "Deep-Learning Methods for Parallel Magnetic Resonance Imaging Reconstruction," *IEEE Signal Process. Mag.*, vol. 37, no. 1, pp. 128–140, 2020.
17. M. Uecker et al., "ESPIRiT—An Eigenvalue Approach to Autocalibrating Parallel MRI," *Magn. Reson. Med.*, vol. 71, no. 3, pp. 990–1001, 2014.
18. S. Boyd et al., "Distributed Optimization and Statistical Learning via the Alternating Direction Method of Multipliers," *Foundations and Trends in Machine Learning*, vol. 3, no. 1, pp. 1–122, 2011.
19. C. A. Metzler, A. Maleki, and R. G. Baraniuk, "From Denoising to Compressed Sensing," *IEEE Trans. Inf. Theory*, vol. 62, no. 9, pp. 5117–5144, 2016.
20. C. A. Metzler, A. Maleki, and R. G. Baraniuk, "Learned D-AMP: Principled Neural Network Based Compressive Image Recovery," in *Proc. NeurIPS*, 2016.
21. K. Chaloner and I. Verdinelli, "Bayesian Experimental Design: A Review," *Statistical Science*, vol. 10, no. 3, pp. 273–304, 1995.
22. A. C. Atkinson, A. N. Donev, and R. D. Tobias, *Optimum Experimental Designs, with SAS*, Oxford University Press, 2007.
23. D. V. Lindley, "On a Measure of the Information Provided by an Experiment," *Annals of Mathematical Statistics*, vol. 27, no. 4, pp. 986–1005, 1956.
24. B. Settles, "Active Learning Literature Survey," University of Wisconsin–Madison, Tech. Rep. 1648, 2009.
25. A. Krause and C. Guestrin, "Near-Optimal Observation Selection Using Submodular Functions," in *Proc. AAAI*, 2008.
26. K. Kandasamy et al., "Neural Architecture Search with Bayesian Optimisation and Optimal Transport," in *Proc. NeurIPS*, 2018.
27. Y. Chen et al., "Active Acquisition for Accelerated MRI Using Deep Reinforcement Learning," *Magn. Reson. Med.*, vol. 85, no. 5, pp. 2824–2837, 2021.
28. J. B. Rawlings, D. Q. Mayne, and M. Diehl, *Model Predictive Control: Theory, Computation, and Design*, 2nd ed., Nob Hill Publishing, 2017.
29. D. Hafner et al., "Dream to Control: Learning Behaviors by Latent Imagination," in *Proc. ICLR*, 2020.
30. A. Jaegle et al., "Perceiver: General Perception with Iterative Attention," in *Proc. ICML*, 2021.
31. J. Zbontar et al., "fastMRI: An Open Dataset and Benchmarks for Accelerated MRI," *arXiv:1811.08839*, 2018.
32. L. Weizman et al., "Deep Learning for Accelerated MRI: Enhanced Reconstruction Using Uncertainty Estimation," *IEEE Trans. Med. Imaging*, vol. 39, no. 6, pp.

ICCS Camera Ready Version 2026
To cite this paper please use the final published version:
DOI: 10.1007/978-3-032-29912-3_32

1987–1997, 2020.
33. H. Chung et al., "Diffusion Models for Inverse Problems in Imaging," *IEEE Trans. Pattern Anal. Mach. Intell.*, 2023.
34. Z. Wang et al., "Image Quality Assessment: From Error Visibility to Structural Similarity," *IEEE Trans. Image Process.*, vol. 13, no. 4, pp. 600–612, 2004.
35. V. Antun et al., "On Instabilities of Deep Learning in Image Reconstruction and the Potential Costs of AI," *Proc. Natl. Acad. Sci. USA*, vol. 117, no. 48, pp. 30088–30095, 2020.
36. L. Pineda et al., "Active Acquisition for Accelerated MRI," in *Proc. MICCAI*, 2019.
37. J. Zhang et al., "On the Role of LORAKS Priors in Adaptive MRI Sampling," *Magn. Reson. Med.*, vol. 82, no. 4, pp. 1518–1532, 2019.
38. J. Chen et al., "TransUNet: Transformers Make Strong Encoders for Medical Image Segmentation," *arXiv:2102.04306*, 2021.

ICCS Camera Ready Version 2026
To cite this paper please use the final published version:
DOI: 10.1007/978-3-032-29912-3_32